International Atomic Energy Agency

INDC(AUS)-011/LI
INT(86)-6

INDC INTERNATIONAL NUCLEAR DATA COMMITTEE

CALCULATION OF THE ENERGY SPREAD AND THE AVERAGE NEUTRON ENERGY OF 14 MeV NEUTRONS PRODUCED VIA THE $T(d,n)^4He$ REACTION IN SOLID TI-T TARGETS

Andreas Pavlik and Gerhard Winkler
Institut für Radiumforschung und Kernphysik der Universität Wien
und der österr. Akademie der Wissenschaften

July 1986

IAEA NUCLEAR DATA SECTION, WAGRAMERSTRASSE 5, A-1400 VIENNA

INDC(AUS)-011/LI
INT(86)-6

CALCULATION OF THE ENERGY SPREAD AND THE AVERAGE NEUTRON ENERGY OF 14 MeV NEUTRONS PRODUCED VIA THE $T(d,n)^4He$ REACTION IN SOLID TI-T TARGETS

Andreas Pavlik and Gerhard Winkler
Institut für Radiumforschung und Kernphysik der Universität Wien
und der österr. Akademie der Wissenschaften

July 1986

Abstract

A Monte Carlo code was developed in order to calculate the energy distribution profile of 14 MeV neutrons produced via the $T(d,n)^4He$ reaction with solid titanium-tritium targets. The slowing down and the angular straggling of the deuterons in the target as well as the finite size of the irradiated sample and the neutron source are taken into account.

Reproduced by the IAEA in Austria
September 1986

86-04072

1. Introduction

The nuclear reaction $T(d,n)^4He$ is widely used as a neutron source for various experiments in basic and applied nuclear physics. Cockcroft-Walton accelerators with the deuterons bombarding solid targets of tritium occluded in metal layers of titanium, yttrium or zirconium work as "neutron generators" in many laboratories providing neutrons with energies around 14 MeV. Typical values of the incident deuteron energy are 150 keV to 250 keV. For example, at 200 keV incident deuteron energy the resulting neutron energy in the laboratory system ranges from 13.18 MeV to 15.09 MeV, dependent on the angle of neutron emission relative to the direction of the incident deuterons.

For an accurate analysis of experimental neutron cross section data the precise value of the average effective neutron energy and its uncertainty as well as the energy distribution of the incident neutrons is required (see e.g. Ref. /1/). Without further corrections the measured cross section can be different from the true microscopic cross section at the average neutron energy due to neutron energy spread effects, even if the excitation function is quite smooth and no sharp resonances occur /1,2/. The influence of the neutron energy distribution profile on the results of an experiment depends on the shape of that distribution. In general such a distribution cannot be described by a single parameter, as e.g. in the case of a Gaussian or a rectangular distribution. But often a single value describing the "energy resolution" is handy in experiment reporting. An appropriate and commonly used quantity is the full width at half maximum (FWHM) of the neutron energy distribution profile, or $\pm \frac{1}{2}$ (FWHM). In order to correctly determine the FWHM one again needs an estimate of the distribution profile.

The Monte Carlo method was chosen to calculate energy distribution profiles for neutrons from the $T(d,n)^4He$ source reaction, for incident deuteron energies from 150 keV to 250 keV, titanium-tritium targets and various irradiation geometries. By means of a digital computer this method effectively makes it feasible to simulate the properties of the deuteron transport in the target layer and to sort and weight the energies of the source neutrons properly.

2. Contributions to the energy spread

The kinetic neutron energy E_n in the laboratory system results from the instantaneous projectile deuteron energy E_d and the angle of neutron emission, Θ, according to the reaction kinematics. The functional dependence of the neutron energy on the neutron emission angle is shown in Fig. 1 for several deuteron energies. Deuterons hitting the target with an incident energy E_{do} are slowed down to zero energy within a titanium-tritium target thicker than the range of these deuterons. (In the following the notation "thick" is used for a target where all deuterons are stopped within the titanium-tritium layer.) For a typical target there exists a tritium-depleted surface layer, the energy loss in which is ΔE_d, such that deuterons with energies from $(E_{do}-\Delta E_d)$ to zero energy contribute to the neutron production. The total neutron yield produced by deuterons in the energy interval (E_d, E_d+dE_d) is proportional to $\sigma(E_d)c(E_d)((dE/dx)(E_d))^{-1}.dE_d$; $\sigma(E_d)$ is the $T(d,n)^4He$ cross section, $c(E_d)$ the tritium concentration, $dE/dx(E_d)$ the specific energy loss of these deuterons, which can be derived from the stopping powers of deuterons in titanium and tritium and the tritium-to-titanium ratio according to Bragg's rule (see, e.g., Refs. /3,4/). If the slowing down of the deuterons is considered only, the average neutron energy $\langle E_n \rangle$ for a given neutron emission angle Θ is:

$$\langle E_n \rangle = \frac{\int_{E_{do}-\Delta E_d}^{o} E_n(E_d,\Theta)\sigma(E_d)c(E_d)((dE/dx)(E_d))^{-1}f(E_d,\Theta)dE_d}{\int_{E_{do}-\Delta E_d}^{o} \sigma(E_d)c(E_d)((dE/dx)(E_d))^{-1}f(E_d,\Theta)dE_d} \tag{1}$$

with $f(E_d,\Theta)$ describing the angular distribution (anisotropy) of neutron emission in the laboratory system. Neglecting angular straggling the slowing down of the deuterons gives practically no contribution to the energy spread of the neutrons at an irradiation angle of about 96° since the neutron energy is rather independent on the deuteron energy at this angle (see Fig. 1).

Angular straggling predominantly due to multiple small-angle scattering also occurs during the slowing down of the deuterons in the target. An approximative expression, describing the angular distribution of the particles penetrating some material by a one-sided Gaussian distribution, was given by Fermi /5/ and was reproduced by Marmier and Sheldon /6/. In the case of deuterons scattered by a titanium layer of thickness x, the variance σ^2 of this distribution which is equal to the mean squared scattering angle relative to the original incident deuteron direction, becomes

$$\overline{\vartheta^2} = \sigma^2 = \frac{3.585}{\bar{E}^2} \; x \log(596.1 \; \bar{E}) \qquad (2)$$

with x the layer thickness in cm and $\bar{E}$ the mean deuteron energy within the layer in MeV. The influence of the tritium atoms on the straggling of the deuterons is neglected.

The approximation Equ. (2) describes the functional relationship between the distribution variance, the layer thickness and the deuteron energy quite simply, but provides two high values for $\overline{\vartheta^2}$ /7/. Neutron energy distribution profiles for relatively thin layers of 40-150 keV for a neutron emission angle of 96° and pointlike sources were calculated using the above approximation. The resulting distributions which were affected only by the angular straggling of the deuterons were compared with the results given by Breunlich /8,9/ based on more sophisticated theories /10,11/, and a normalization factor for the right side of Equ. (2) was derived. For incident deuteron energies between 150 keV and 250 keV the normalization factor was found to be 0.285 with an uncertainty of about ± 0.014.

For incident deuteron energies around 200 keV it has been suggested /8/ to describe the scattering of the deuterons globally by a Gaussian distribution with a FWHM of 14° neglecting the deuteron energy dependent broadening of the scattering cone during the slowing-down process. This assumption of a global distribution was found to work almost as well as taking into account the energy dependence according to Equ. (2) for incident deuteron energies close to 200 keV when comparing calculated neutron energy profiles using both models.

A third contribution to the neutron energy spread results from the spread in neutron emission angles due to the finite size of the sample and the beamspot. When using extended samples (e.g. long cylinders, see Fig. 3) the variation of the distance beamspot to sample-volume element along the sample has to be considered additionally. Both the deuteron straggling and the finite solid angle subtended by the sample with respect to the neutron source significantly contribute to the width of the final neutron energy distributions at irradiation angles around 96° according to the slope of the functional dependence neutron energy versus neutron emission angle.

The most proper way to calculate the final neutron energy distribution profiles for a variety of irradiation geometries and irradiation angles seemed to be the Monte Carlo method. All contributions to the energy spread can be taken into account simultaneously as they physically occur; therefore all existing correlations are then considered automatically. This procedure avoids the problems encountered in a different method to obtain the total energy resolution in an experiment from separately estimated distribution widths for the various contributions to the final energy spread, i.e. how to properly combine the corresponding distribution parameters. Adding the partial FWHMs in quadrature in order to get the total FWHM would be correct if all distributions involved were Gaussian and correlations amongst these contributions could be neglected. Standard deviations may however be added in quadrature regardless of the shape of the distributions if, again, no correlations exist. The latter is certainly not fullfilled for the partial processes contributing to the total energy spread of the produced neutrons.

3. The Code PROFIL

The neutron energy distribution profiles using thick titanium-tritium targets are calculated by means of the Monte Carlo code PROFIL for different experimental setups used at the Institut für Radiumforschung und Kernphysik (IRK), Vienna. In activation experiments the samples employed are usually thin foils (disc-shaped or rectangular) positioned at various distances and irradiation angles (as, e.g., in Fig. 2). The deuteron beamspot is assumed to be circular and homogeneous regarding beam intensity. Neutron scattering in the target backing (0.3 mm thick copper at IRK) and in the low-mass target-holder construction is not considered here. Its influence has to be taken into account depending on the shape of the excitation functions for the cross sections under study (see e.g. Refs. /12,13/). In time-of-flight experiments, in order to measure energy and angular distributions of secondary neutrons, larger cylindrical samples of typically 12 cm in length and 2 cm in diameter (Fig. 3) are used.

In each history, numbered by the index i, the energy E_{ni} of a neutron incident on the sample and a corresponding weight w_i are calculated. The source coordinates and the coordinates of the point of interaction between the neutron and the sample are chosen by random sampling on the basis of equidistribution within the circular beamspot and within the sample volume, respectively.

The energy E_{di} of the deuteron interacting with tritium is taken randomly from the interval $(E_{do}-\Delta E_d,0)$. In order to calculate the variance of the angular distribution of the deuterons slowed down to the energy E_{di} according to Equ. (2), the path length $x_i(E_{di})$ and the mean deuteron energy $\bar{E}(E_{di})$ are interpolated from previously established tables. The scattering angle ϑ_i is chosen from a one-sided normal distribution generating normally distributed random numbers by the polar method /14/. The range of the ϑ_i values is restricted to the interval $(0, 3\sqrt{\sigma^2})$, with σ^2 taken according to Equ. (2), disregarding histories with larger ϑ_i values. After the value of the azimuthal angle φ_i has been chosen (taken as to be equidistributed), the direction of the scattered deuteron and therefore the neutron emission angle Θ_i (see Fig. 4) are fixed, as the direction of the emitted neutron is given by the coordinates of the source and sample elements. The neutron energy in the laboratory system $E_{ni}(E_{di},\Theta_i)$ and the yield anisotropy factor $f_i(E_{di},\Theta_i)$ are calculated for every history according to relativistic reaction kinematics. Since the $T(d,n)^4He$ reaction can be assumed to be isotropic in the center of mass reference frame in the energy range considered, the anisotropy factor $f_i(E_{di},\Theta_i)$ is determined by the ratio of the solid angles in the center of mass system to those in the laboratory system. The stopping power $(dE/dx)(E_{di})$, the tritium concentration $c(E_d)$ and the source reaction cross section $\sigma(E_{di})$ are interpolated from tables. The weight factor w_i is given by

$$w_i = \sigma(E_{di}).c(E_{di}).((dE/dx)(E_{di}))^{-1}.f(E_{di},\Theta_i)/d_i^2 \qquad (3)$$

with d_i the distance between the source and the sample element.

The average neutron energy results as the weighted average:

$$\bar{E}_n = \sum_i w_i E_{ni} / \sum_i w_i \qquad (4)$$

In order to calculate the energy distribution profile the neutron energy scale is divided into bins of equal width (usually 10 keV) and the neutron energies E_{ni} are sorted into these bins. Summing up the weight factors w_i for all energies fitting in the limits of each energy bin yields a histogram which represents the neutron energy distribution profile. The standard deviation of the neutron energies is calculated simultaneously with the average neutron energy, the FWHM has to be derived from the neutron energy distribution profile.

The stopping power values for titanium and tritium are taken from Ref. /15/ and are combined according to the tritium-to-titanium ratio, the $T(d,n)^4He$ reaction cross sections are taken from Ref. /16/.

The Code PROFIL is written in FORTRAN 77 and runs on a PDP 11/34 or a VAX 11/750 computer.

4. Results and discussion

The calculated effective neutron energy distribution profiles (20 000 histories each) for incident deuteron energies of 150, 175, 200 and 220 keV (the latter is most common at IRK) and samples positioned at irradiation angles 0°, 30°, 60°, 100°, 120° and 150° are shown in Figs. 5 to 8. (As for a target mounted normally to the deuteron beam (see Fig. 2) an irradiation angle of 90° cannot be used in practice, an irradiation angle of 100° was chosen instead.) All calculations were performed for thick titanium-tritium targets, assuming 10 keV deuteron energy loss in a tritium-depleted front layer and a tritium-to-titanium ratio of 1.5, which was taken to be constant throughout the whole thickness of the effective target material. Thin discs were chosen as the samples, 2 cm in diameter, at a distance of 10 cm from the beamspot, which was taken to be 0.8 cm in diameter. All neutron energy distributions shown in the figures are normalized to equal areas. The neutron energy profiles shown deviate significantly from a Gaussian shape in most cases. They tend to become asymmetric for neutrons emitted in the forward and backward direction, with the tails of the distributions extending to lower energies in the forward direction and to higher energies in the backward direction. These tails are caused by the slowing-down of the deuterons and the dependence of the neutron energy on the reaction angle becoming rather flat with decreasing deuteron energy (see Fig. 1). A symmetric spread of the neutron emission angle due to the finite geometry and the small-angle scattering also causes asymmetry of the neutron energy profiles on basis of the shape of the kinematic relationship neutron energy versus emission angle (Fig. 1). An extreme situation occurs at an irradiation angle of 0°, where a variation of the emission angle results in a decreasing neutron energy in any case leading to a rather sharp edge at the high-energy end of the profile.

The average neutron energy, the standard deviation and the FWHM of the calculated neutron energy profiles, and the ratio of the FWHM to the standard deviation are summarized in Table 1.

As can be gathered from the table, in several cases the ratio FWHM/σ is significantly different from 2.35, a value which would result in case of a normal distribution.

The neutron energy profiles shown in Figs. 9a,b and 10a,b are intended to demonstrate the situation in case of an irradiation angle of 96°, where the neutron energy is rather independent on the deuteron energy (see Fig. 1). The distributions in Fig. 9a and b have been obtain-

Table 1 Average neutron energy $\bar{E}_n$, standard deviation σ, FWHM, and the ratio σ/FWHM, for the neutron energy distribution profiles calculated with the Monte Carlo code PROFIL, for various incident deuteron energies E_{do} and irradiation angles Θ.

Θ (deg)	$\bar{E}_n$ (MeV)	σ (MeV)	FWHM (MeV)	FWHM/σ
		E_{do} = 150 keV		
0	14.727	0.118	0.286	2.42
30	14.637	0.108	0.270	2.50
60	14.392	0.082	0.186	2.27
100	13.953	0.056	0.125	2.23
120	13.746	0.063	0.139	2.21
150	13.517	0.080	0.177	2.21
		E_{do} = 175 keV		
0	14.767	0.135	0.383	2.84
30	14.672	0.123	0.327	2.66
60	14.415	0.091	0.220	2.42
100	13.951	0.059	0.129	2.19
120	13.733	0.067	0.152	2.27
150	13.493	0.089	0.223	2.51
		E_{do} = 200 keV		
0	14.801	0.152	0.442	2.91
30	14.701	0.138	0.386	2.80
60	14.432	0.100	0.251	2.51
100	13.949	0.060	0.132	2.20
120	13.724	0.071	0.171	2.41
150	13.473	0.099	0.268	2.71
		E_{do} = 220 keV		
0	14.823	0.166	0.490	2.95
30	14.723	0.149	0.439	2.95
60	14.444	0.107	0.281	2.63
100	13.950	0.062	0.139	2.24
120	13.717	0.075	0.171	2.28
150	13.460	0.105	0.283	2.70

ed with the variance of the small-angle scattering distribution set to zero. (The incident deuteron energy was taken to be 200 keV, the thickness of the tritium depleted front layer 10 keV, and the tritium-to-titanium ratio 1.5 throughout the target.) The beamspot was assumed to be small (2 mm in diameter) thus that a major contribution to the neutron energy spread could stem from the finite size of the samples only. As the sample a disc of 0.5 cm and 2 cm in diameter, each at a distance of 10 cm from the TiT target, was taken for Fig. 9a and Fig. 9b, respectively.

Figures 10a and 10b show the neutron energy profiles calculated under the same conditions as for Figs. 9a and 9b, but with the effect of the angular straggling of the deuterons included. These figures demonstrate the limits of energy resolution that can be obtained even if small samples at kinematically preferable irradiation angles are chosen. For an irradiation angle of 96° deuteron scattering provides effective neutrons emitted at angles different from 96°, where the neutron energy is not independent on the deuteron energy. This is a plain example showing that straggling and slowing down of the deuterons cannot be treated as independently affecting the distribution profiles.

All the calculations mentioned above were performed on the assumption that there is no ripple on the accelerating voltage, otherwise this would cause a possible additional spread of the neutron energy.

5. The uncertainty of the average neutron energy

Apart from the necessity to determine the neutron energy spread, an estimate of the uncertainty of the average energy is needed. The uncertainty of the average energy is determined by the uncertainties of the input parameters entering into the model used to calculate the neutron energy profiles. The principal sources of uncertainty of the effective mean neutron energy are the uncertainties in the incident deuteron energy, the Q value of the $T(d,n)^4He$ reaction, the deuteron energy loss in a tritium-depleted front layer, the actual tritium concentration profile, the specific energy loss of the deuterons in the target, the shape of the neutron production cross section /16/ and the angular position of the sample. In practice the most significant contributions to the uncertainty of the mean neutron energy will stem from the deuteron energy loss in the tritium-depleted front layer, which was assumed to be 10 ± 10 keV (see, e.g., Ref. /4/) and the positioning of the sample. The tritium-to-titanium ratio (assumed to be 1.5 ± 0.5) and reasonable variations of the tritium concentration profile have only a slight effect on the average neutron energy. Taking additionally into account the uncertainty of stopping power data for the deuterons (which causes an uncertainty in the average neutron energy of ± 3 keV, at the most, when comparing the results using different literature values from Refs. /3, 15, 17/ for the specific energy loss) and an uncertainty of ±1° in the sample position, results in the uncertainties of the average neutron energies, $\bar{E}_n$, already calculated in section 4. They are listed in Table 2

Table 2 Average neutron energy $\bar{E}_n$, calculated by means of the Monte Carlo code PROFIL, together with its uncertainty, compared with the average neutron energy values $\langle E_n \rangle$ as obtained according to Equ. (1).

θ (deg)	$\bar{E}_n$ (MeV)	$\langle E_n \rangle$ (MeV)
	E_{do} = 150 keV	
0	14.727 ± 0.019	14.734
30	14.637 ± 0.017	14.642
60	14.392 ± 0.014	14.395
100	13.953 ± 0.012	13.952
120	13.746 ± 0.012	13.742
150	13.517 ± 0.013	13.511
	E_{do} = 175 keV	
0	14.767 ± 0.015	14.774
30	14.672 ± 0.015	14.677
60	14.415 ± 0.014	14.416
100	13.951 ± 0.019	13.950
120	13.733 ± 0.012	13.730
150	13.493 ± 0.011	13.488
	E_{do} = 200 keV	
0	14.801 ± 0.013	14.807
30	14.701 ± 0.014	14.706
60	14.432 ± 0.014	14.435
100	13.949 ± 0.013	13.949
120	13.724 ± 0.012	13.720
150	13.473 ± 0.010	13.468
	E_{do} = 220 keV	
0	14.823 ± 0.012	14.831
30	14.723 ± 0.012	14.723
60	14.444 ± 0.013	14.447
100	13.950 ± 0.013	13.948
120	13.717 ± 0.011	13.713
150	13.460 ± 0.010	13.455

which for comparison also comprises the mean neutron energies, $\langle E_n \rangle$, obtained by numerical evaluation of the integrals on the right side of Equ. (1).

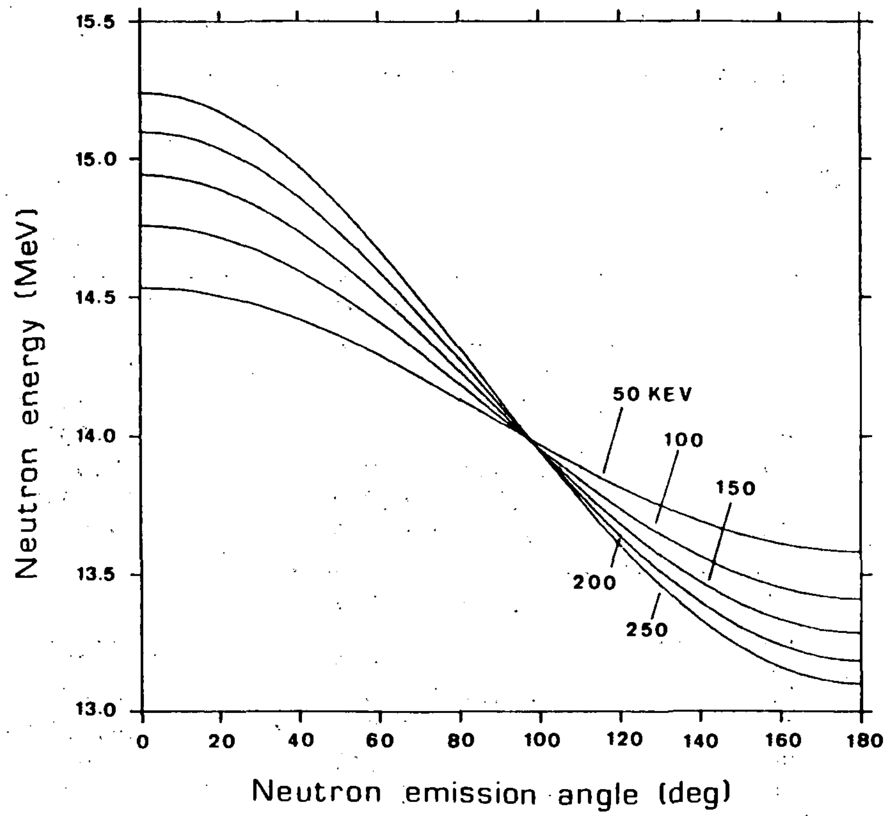

Fig. 1. The kinetic laboratory system energy of $T(d,n)^4He$ neutrons as a function of the laboratory angle of neutron emission for deuteron energies from 50 to 250 keV

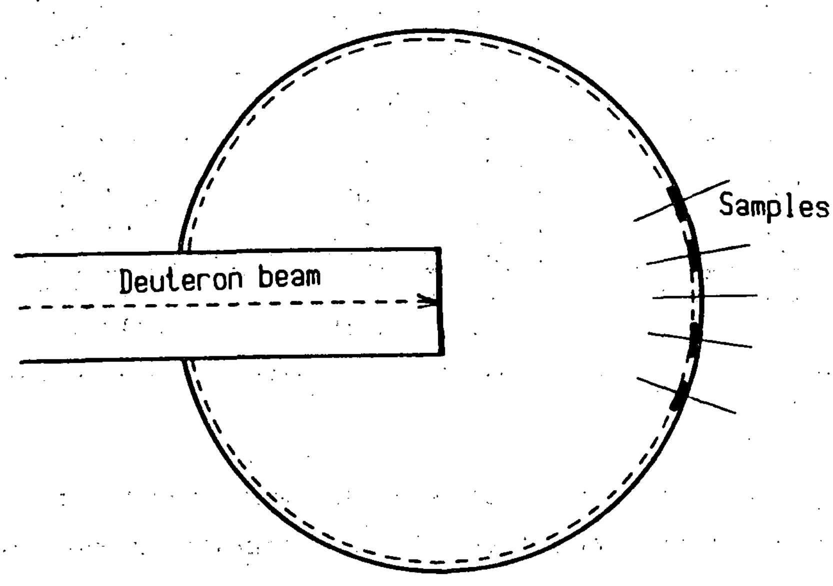

Fig. 2. Irradiation geometry for activation experiments

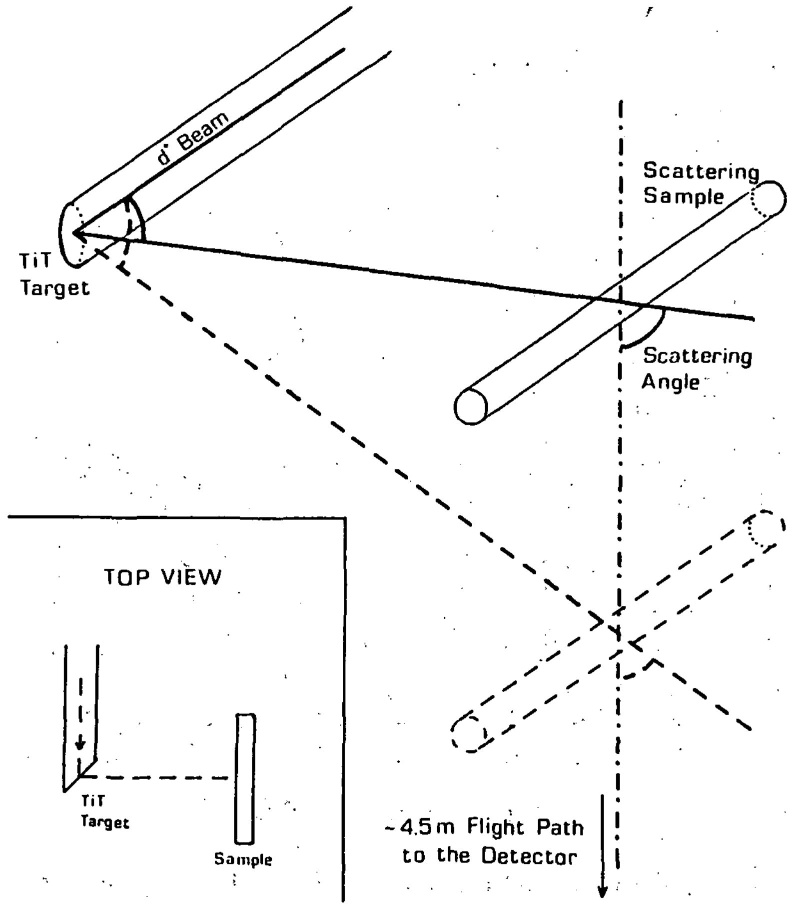

Fig. 3. Irradiation geometry for time-of-flight experiments to measure energy- and angular differential secondary neutron emission cross sections. (The scattering angle is changed by moving the sample along the neutron detector axis.)

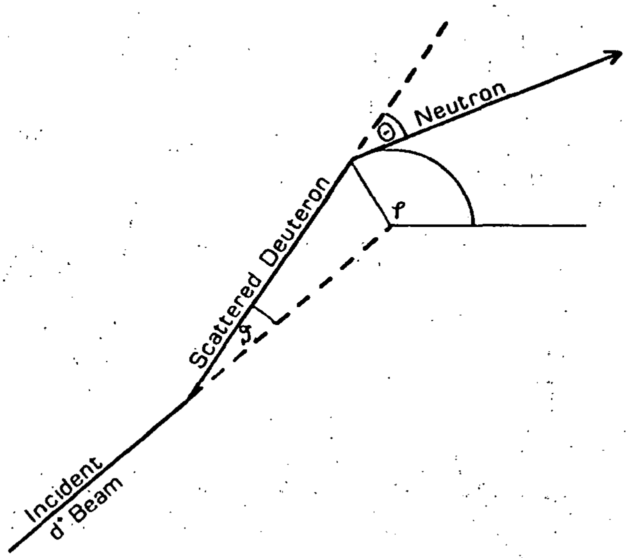

Fig. 4. Determination of the angle Θ of neutron emission in the laboratory system

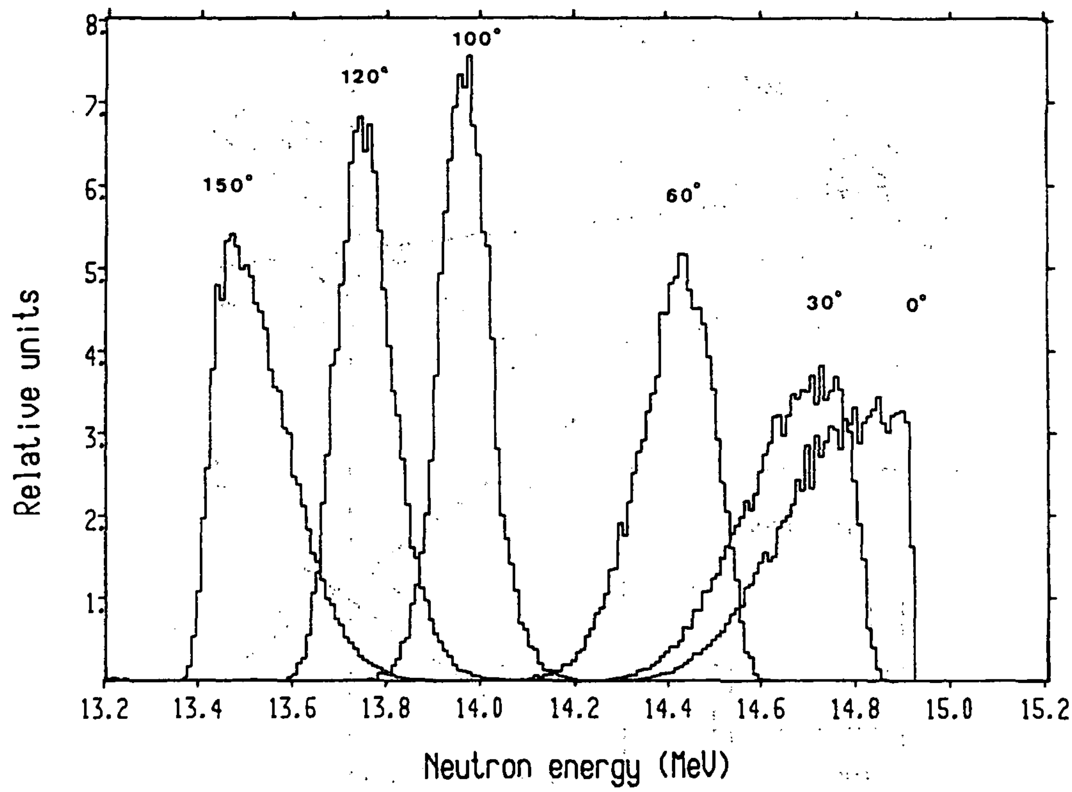

Fig. 5. The neutron energy distribution profiles at an energy of 150 keV of the bombarding deuterons for various irradiation angles relative to the neutron generator axis.

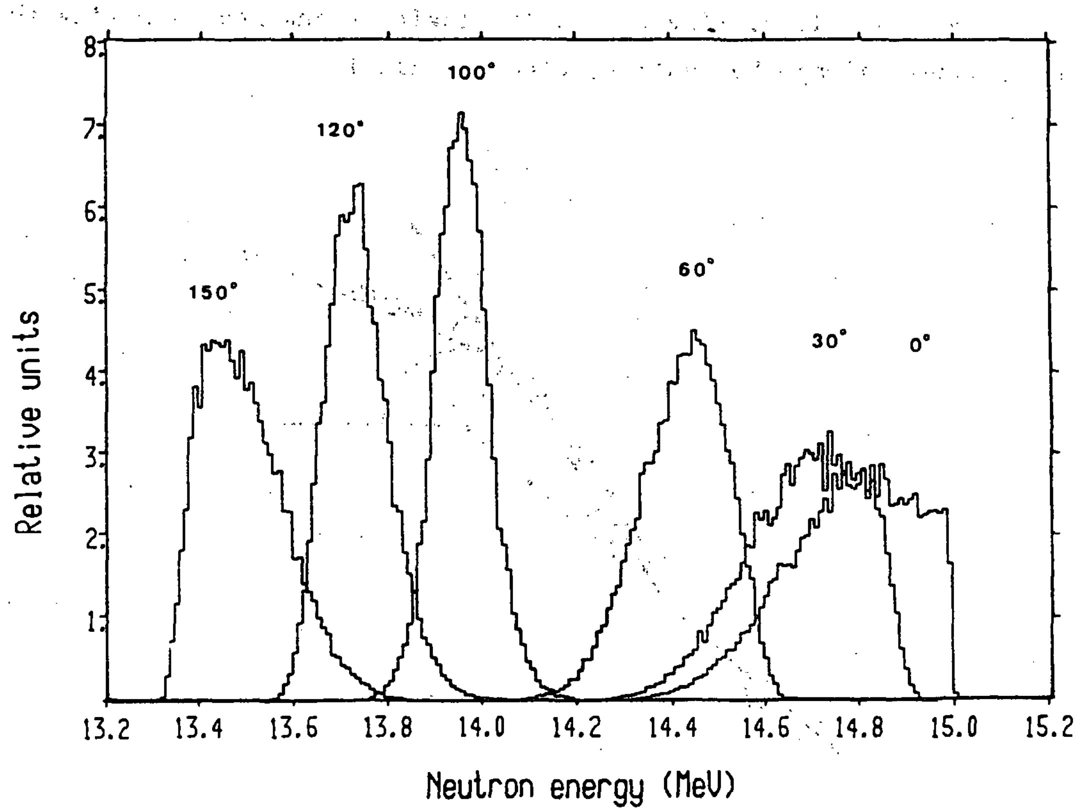

Fig. 6. The neutron energy distribution profiles at an incident deuteron energy of 175 keV for various irradiation angles

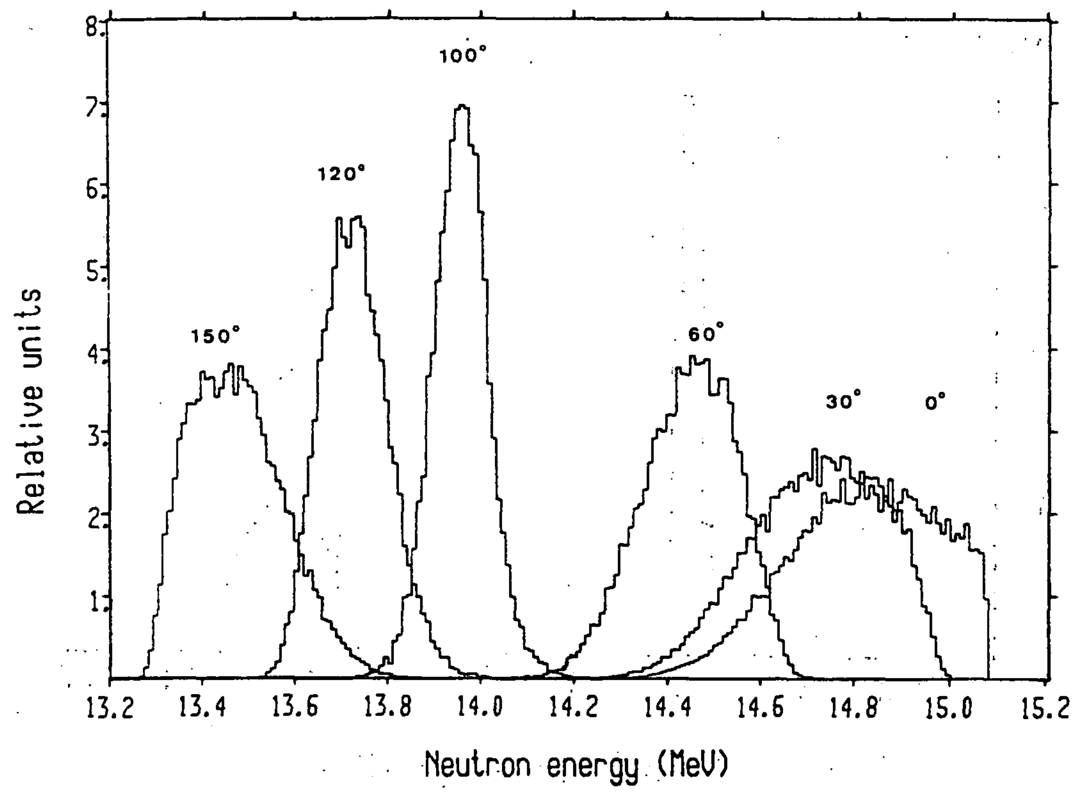

Fig. 7. The neutron energy distribution profiles at an incident deuteron energy of 200 keV for various irradiation angles

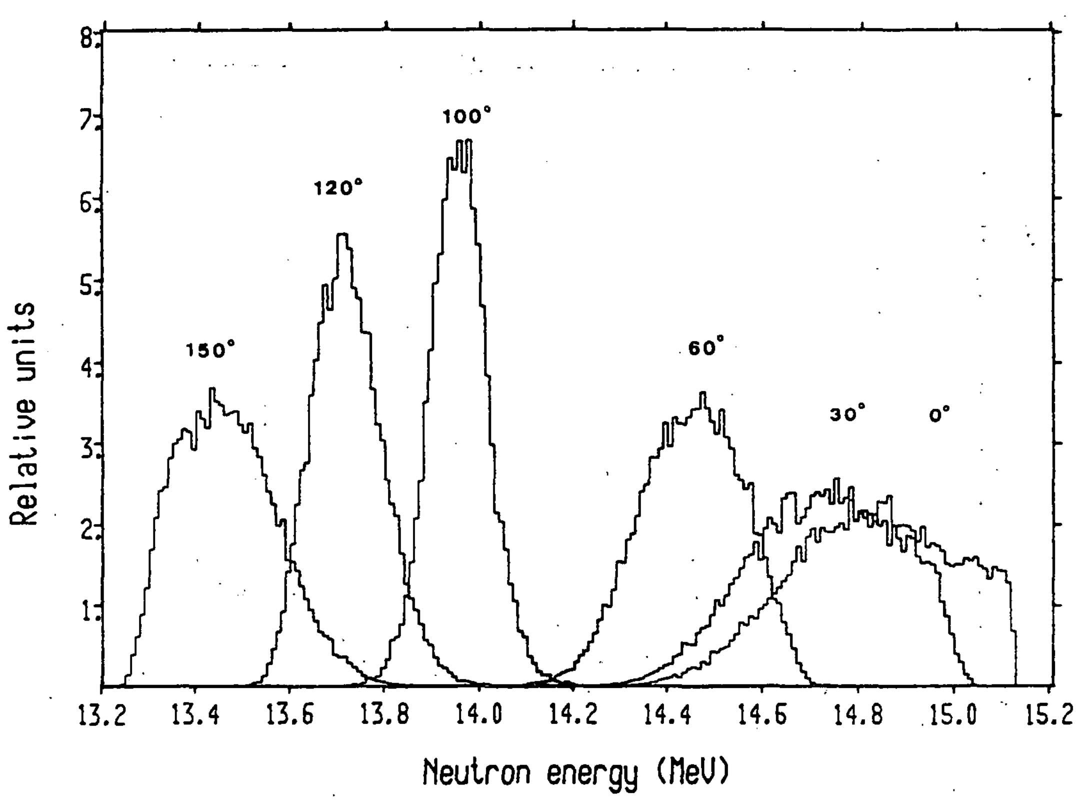

Fig. 8. The neutron energy distribution profiles at an incident deuteron energy of 220 keV for various irradiation angles

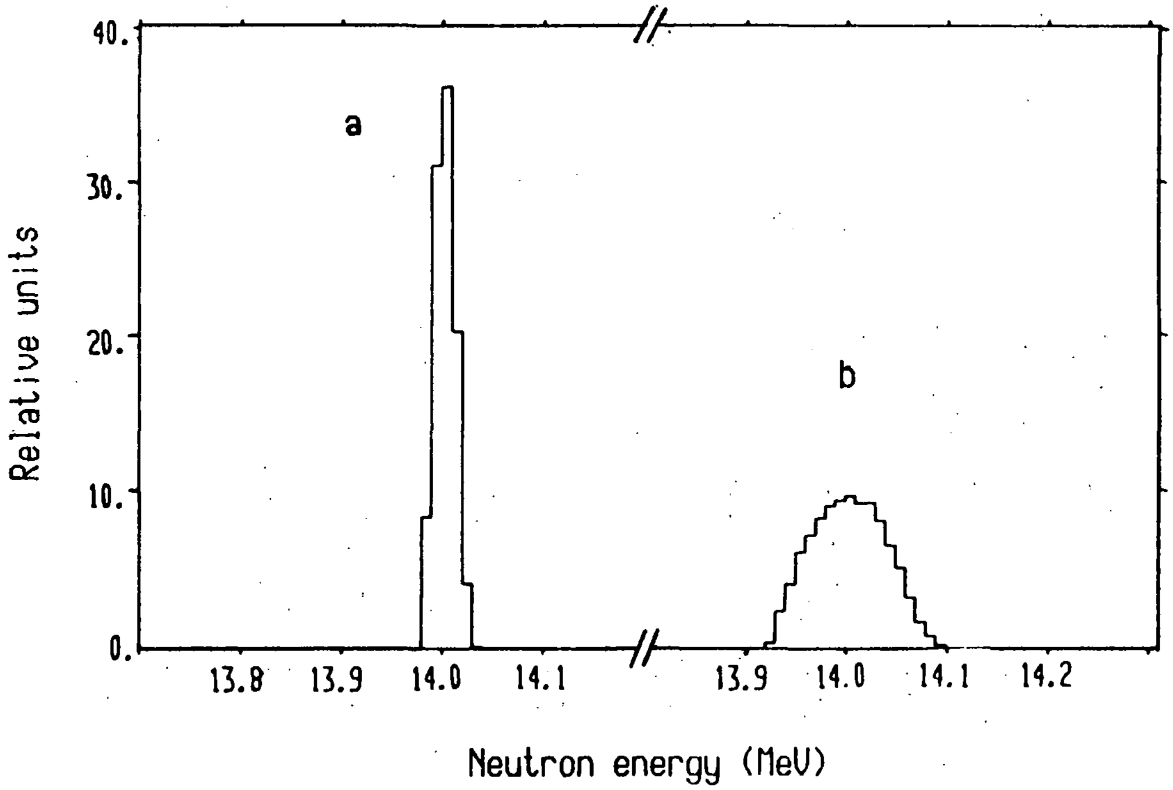

Fig. 9. The neutron energy distribution profiles at 200 keV incident deuteron energy and an irradiation angle of 96° with deuteron scattering neglected for different solid angles subtended by the sample

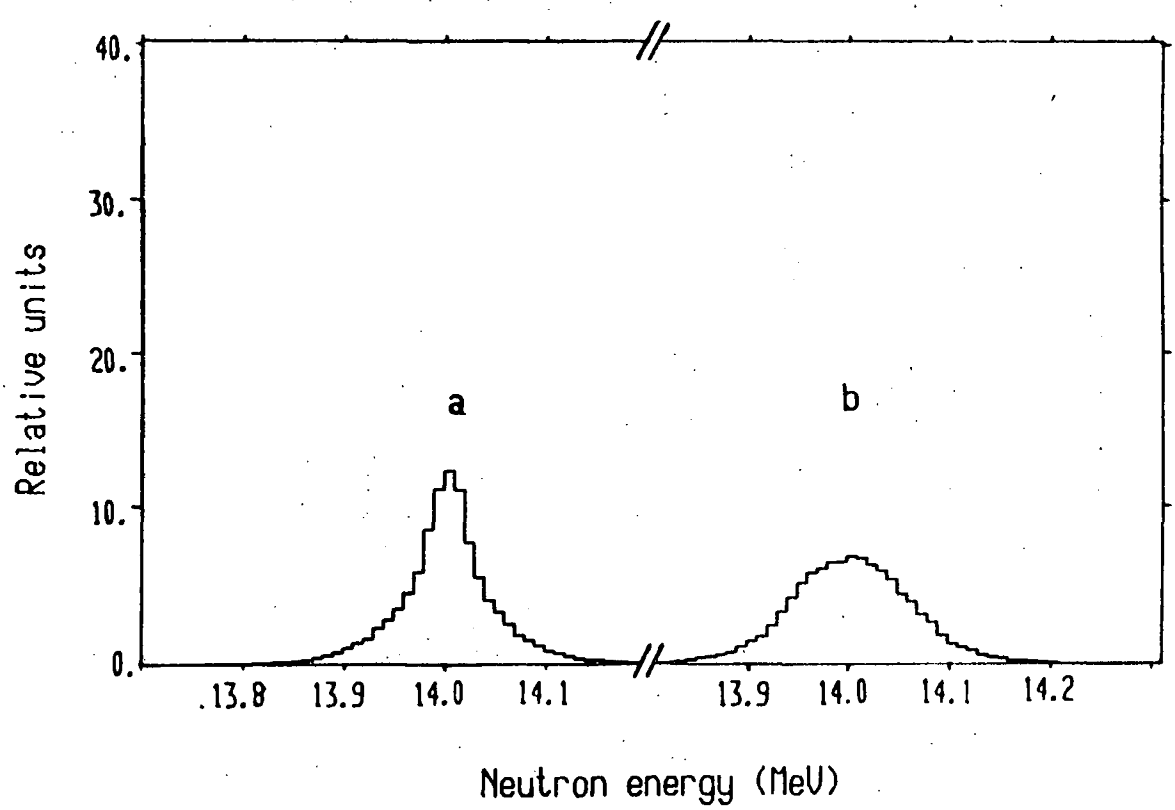

Fig. 10. The neutron energy distribution profiles under the same conditions as in Fig. 9., but with deuteron scattering included

References

/1/ D.L. Smith, "Some comments on resolution and analysis and interpretation of experimental results from differential neutron measurements", Report ANL/NDM-49, Argonne National Laboratory, Argonne 1979

/2/ G. Winkler, D.L. Smith, J.W. Meadows, Nucl. Sci. Eng. 76, 30 (1980)

/3/ T.R. Fewell, Nucl. Instr. and Meth. 61, 61 (1968)

/4/ E.M. Gunnersen and G. James, Nucl. Instr. and Meth. 8, 173 (1960)

/5/ E. Fermi, Nuclear Physics (Notes compiled by J. Orear, A.M. Rosenfeld and R.A. Schluter), University of Chicago Press, Chicago 1950

/6/ P. Marmier, E. Sheldon, Physics of Nuclei and Particles, vol. I, p. 155, Academic Press, New York 1969

/7/ H. Klein, H.J. Brede, B.R.L. Siebert, Nucl. Instr. and Meth. 193, 635 (1982)

/8/ W.H. Breunlich, Sitzungsberichte d. Österr. Akad. Wiss., math.-naturw. Kl., Abt. II, 175, 1 (1966)

/9/ W.H. Breunlich, Acta Phys. Austr. 23, 224 (1966)

/10/ W.T. Scott, Rev. Mod. Phys. 35, 231 (1963)

/11/ G. Molière, Z. Naturf. 2a, 133 (1947)
Z. Naturf. 3a, 78 (1948)

/12/ A. Pavlik, G. Winkler, H. Vonach, A. Paulsen and H. Liskien, J. Phys. G: Nucl. Phys. 8, 1283 (1982)

/13/ A. Pavlik, G. Winkler, M. Uhl, A. Paulsen and H. Liskien, Nucl. Sci. Eng. 90, 186 (1985)

/14/ D.E. Knuth, The Art of Computer Programming, vol. 2, p. 103, Addison-Wesley, Reading, Mass. 1969

/15/ H.H. Andersen and J.F. Ziegler, Hydrogen Stopping Powers and Ranges in All Elements (vol. 3 of J.F. Ziegler ed., The Stopping and Ranges of Ions in Matter), Pergamon Press, New York 1977

/16/ H. Liskien, A. Paulsen, Nuclear Data Tables 11, 569 (1973)

/17/ J.H. Ormrod, Nucl. Instr. and Meth. 95, 49 (1971)